Simultaneous measurement of pressure and temperature by employing Fabry-Perot interferometer based on pendant polymer droplet

Bing Sun,[1] Yiping Wang,[1,2] Junle Qu,[1,3] Changrui Liao,[1] Guolu Yin,[1] Jun He,[1] Jiangtao Zhou,[1] Jian Tang,[1] Shen Liu,[1] Zhengyong Li,[1] and Yingjie Liu[1]

[1]*Key Laboratory of Optoelectronic Devices and Systems of Ministry of Education and Guangdong Province, College of Optoelectronic Engineering, Shenzhen University, Shenzhen 518060, China*
[2]*ypwang@szu.edu.cn*
[3]*jlqu@szu.edu.cn*

Abstract: We investigated a novel and ultracompact polymer-capped Fabry-Perot interferometer, which is based on a polymer capped on the endface of a single mode fiber (SMF). The proposed Fabry-Perot interferometer has advantages of easy fabrication, low cost, and high sensitivity. The variation of the Fabry-Perot cavity length can be easily controlled by using the motors of a normal arc fusion splicer. Moreover, the enhanced mechanical strength of the Fabry-Perot interferometer makes it suitable for high sensitivity pressure and temperature sensing in harsh environments. The proposed interferometer exhibits a wavelength shift of the interference fringes that corresponds to a temperature sensitivity of 249 pm/°C and a pressure sensitivity of 1130 pm/MPa, respectively, around the wavelength of 1560 nm.

OCIS codes: (060.2370) Fiber optics sensors; (120.2230) Fabry-Perot; (130.3990) Micro-optical devices.

References and links

1. Q. Rong, H. Sun, X. Qiao, J. Zhang, M. Hu, and Z. Feng, "A miniature fiber-optic temperature sensor based on a Fabry–Perot interferometer," J. Opt. **14**(4), 045002 (2012).
2. M. S. Ferreira, J. Bierlich, J. Kobelke, K. Schuster, J. L. Santos, and O. Frazão, "Towards the control of highly sensitive Fabry-Pérot strain sensor based on hollow-core ring photonic crystal fiber," Opt. Express **20**(20), 21946–21952 (2012).
3. F. C. Favero, L. Araujo, G. Bouwmans, V. Finazzi, J. Villatoro, and V. Pruneri, "Spheroidal Fabry-Perot microcavities in optical fibers for high-sensitivity sensing," Opt. Express **20**(7), 7112–7118 (2012).
4. D.-W. Duan, Y.-J. Rao, Y.-S. Hou, and T. Zhu, "Microbubble based fiber-optic Fabry-Perot interferometer formed by fusion splicing single-mode fibers for strain measurement," Appl. Opt. **51**(8), 1033–1036 (2012).
5. J. Villatoro, V. Finazzi, G. Coviello, and V. Pruneri, "Photonic-crystal-fiber-enabled micro-Fabry-Perot interferometer," Opt. Lett. **34**(16), 2441–2443 (2009).
6. X. Chen, F. Shen, Z. Wang, Z. Huang, and A. Wang, "Micro-air-gap based intrinsic Fabry-Perot interferometric fiber-optic sensor," Appl. Opt. **45**(30), 7760–7766 (2006).
7. G. Hill, R. Melamud, F. Declercq, A. Davenport, I. Chan, P. Hartwell, and B. Pruitt, "SU-8 MEMS Fabry-Perot pressure sensor," Sens. Actuators A Phys. **138**(1), 52–62 (2007).
8. J. Ma, J. Ju, L. Jin, and W. Jin, "A compact fiber-tip micro-cavity sensor for high-pressure measurement," IEEE Photon. Technol. Lett. **23**(21), 1561–1563 (2011).
9. H. Bae, L. Dunlap, J. Wong, and M. Yu, "Miniature Temperature Compensated Fabry–Perot Pressure Sensors Created With Self-Aligned Polymer Photolithography Process," IEEE Sens. J. **12**(5), 1566–1573 (2012).
10. H. Bae and M. Yu, "Miniature Fabry-Perot pressure sensor created by using UV-molding process with an optical fiber based mold," Opt. Express **20**(13), 14573–14583 (2012).
11. J.-R. Zhao, X.-G. Huang, W.-X. He, and J.-H. Chen, "High-resolution and temperature-insensitive fiber optic refractive index sensor based on fresnel reflection modulated by Fabry–Perot interference," Lightwave Technology, Journalism **28**(19), 2799–2803 (2010).

#222170 - $15.00 USD Received 1 Sep 2014; revised 12 Jan 2015; accepted 19 Jan 2015; published 26 Jan 2015

12. O. Frazão, P. Caldas, J. L. Santos, P. V. Marques, C. Turck, D. J. Lougnot, and O. Soppera, "Fabry-Perot refractometer based on an end-of-fiber polymer tip," Opt. Lett. **34**(16), 2474–2476 (2009).
13. J. Goicoechea, C. Zamarreño, I. Matias, and F. Arregui, "Utilization of white light interferometry in pH sensing applications by mean of the fabrication of nanostructured cavities," Sens. Actuators B Chem. **138**(2), 613–618 (2009).
14. H. Y. Choi, G. Mudhana, K. S. Park, U.-C. Paek, and B. H. Lee, "Cross-talk free and ultra-compact fiber optic sensor for simultaneous measurement of temperature and refractive index," Opt. Express **18**(1), 141–149 (2010).
15. D. J. Hu, J. L. Lim, M. Jiang, Y. Wang, F. Luan, P. P. Shum, H. Wei, and W. Tong, "Long period grating cascaded to photonic crystal fiber modal interferometer for simultaneous measurement of temperature and refractive index," Opt. Lett. **37**(12), 2283–2285 (2012).
16. T. Zhu, Y. Rao, and Q. Mo, "Simultaneous measurement of refractive index and temperature using a single ultra-long-period fiber grating," IEEE Photon. Technol. Lett. **17**(12), 2700–2702 (2005).
17. X. Zhang, Y. Yu, C. Zhu, C. Chen, R. Yang, Y. Xue, Q. Chen, and H. Sun, "Miniature End-Capped Fiber Sensor for Refractive Index and Temperature Measurement," IEEE Photon. Technol. Lett. **26**(1), 7–10 (2014).
18. T. Han, Y. G. Liu, Z. Wang, Z. Wu, S. Wang, and S. Li, "Simultaneous temperature and force measurement using Fabry-Perot interferometer and bandgap effect of a fluid-filled photonic crystal fiber," Opt. Express **20**(12), 13320–13325 (2012).
19. H. Liang, W. Zhang, P. Geng, Y. Liu, Z. Wang, J. Guo, S. Gao, and S. Yan, "Simultaneous measurement of temperature and force with high sensitivities based on filling different index liquids into photonic crystal fiber," Opt. Lett. **38**(7), 1071–1073 (2013).
20. C. Yang, H. Zhang, H. Liang, Y. Miao, B. Liu, Z. Wang, and Y. Liu, "Selectively liquid-infiltrated microstructured optical fiber for simultaneous temperature and force measurement," IEEE Photon. J. **6**(2), 6800808 (2014).
21. J. Villatoro, V. P. Minkovich, and J. Zubia, "Locally pressed photonic crystal fiber interferometer for multiparameter sensing," Opt. Lett. **39**(9), 2580–2583 (2014).
22. S. Pevec and D. Donlagic, "Miniature all-fiber Fabry-Perot sensor for simultaneous measurement of pressure and temperature," Appl. Opt. **51**(19), 4536–4541 (2012).
23. C. Pang, H. Bae, A. Gupta, K. Bryden, and M. Yu, "MEMS Fabry-Perot sensor interrogated by optical system-on-a-chip for simultaneous pressure and temperature sensing," Opt. Express **21**(19), 21829–21839 (2013).
24. H. Bae, D. Yun, H. Liu, D. A. Olson, and M. Yu, "Hybrid Miniature Fabry–Perot Sensor with Dual Optical Cavities for Simultaneous Pressure and Temperature Measurements," J. Lightwave Technol. **32**(8), 1585–1593 (2014).
25. C. Liao, S. Liu, L. Xu, C. Wang, Y. Wang, Z. Li, Q. Wang, and D. N. Wang, "Sub-micron silica diaphragm-based fiber-tip Fabry-Perot interferometer for pressure measurement," Opt. Lett. **39**(10), 2827–2830 (2014).
26. C.-L. Lee, L.-H. Lee, H.-E. Hwang, and J.-M. Hsu, "Highly sensitive air-gap fiber Fabry-Perot interferometers based on polymer-filled hollow core fibers," IEEE Photon. Technol. Lett. **24**(2), 149–151 (2012).
27. Norland Products Inc, *https://www.norlandprod.com/adhesives/NOA%2065.html*
28. Z. L. Ran, Y. J. Rao, W. J. Liu, X. Liao, and K. S. Chiang, "Laser-micromachined Fabry-Perot optical fiber tip sensor for high-resolution temperature-independent measurement of refractive index," Opt. Express **16**(3), 2252–2263 (2008).
29. Y. Wang, "Review of long period fiber gratings written by CO_2 Laser," J. Appl. Phys. **108**(8), 081101 (2010).
30. Y. Wang, Y. J. Rao, and Z. L. Ran, "Unique characteristics of long-period fibre gratings fabricated by high-frequency CO_2 laser pulses," Acta Phys. Sin. **52**, 1432–1437 (2003).
31. K. R. Sohn and G.-D. Peng, "Mechanically formed loss-tunable long-period fiber gratings realized on the periodic arrayed metal wires," Opt. Commun. **278**(1), 77–80 (2007).
32. W. Jin, W. C. Wichie, G. Thursby, M. Konstantaki, and B. Culshaw, "Simultaneous measurement of strain and temperature: Error analysis," Opt. Eng. **36**(2), 598–609 (1997).
33. J. L. Qu, L. X. Liu, Y. H. Shao, H. Niu, and B. Gao, "Recent process in multiofocal multiphoton microscopy," J. Innov. Opt. Heal. Sci. **5**(3), 1250018 (2012).
34. X. Zhang, Y. Xiao, J. Qi, J. Qu, B. Kim, X. Yue, and K. D. Belfield, "Long-wavelength, photostable, two-photon excitable BODIPY fluorophores readily modifiable for molecular probes," J. Org. Chem. **78**(18), 9153–9160 (2013).

1. Introduction

Fiber optic Fabry-Perot interferometric sensors have been extensively investigated and used in various areas of biomedicine, automotive industries, and environmental monitoring due to the advantages of ultra-compact size, high sensitivity, excellent thermal stability, immunity to electromagnetic interference and convenience of light guiding/detection through optical fibers. It is well known that Fabry-Perot interferometric sensors can be used to detect physical and chemical parameters such as temperature [1], strain [2–6], pressure [7–10], refractive index [11–12] and pH [13]. However, the aforementioned sensors are usually confined to single parameter measurement owing to limits of the structure or material. It is noteworthy

#222170 - $15.00 USD Received 1 Sep 2014; revised 12 Jan 2015; accepted 19 Jan 2015; published 26 Jan 2015

that more and more studies have focused on the design of dual-parameter sensors, and the principle of which is often based on the sensing head having different sensitivities to each of two physical parameter, such as temperature-refractive index [14–17], temperature-force [18–21] and temperature-pressure [22–25]. Among these, simultaneous measurement of pressure and temperature is a crucial application of optical dual-parameter sensors. Unfortunately, a costly laser system and reactive-ion-etching technology [23] or complex fabrication technique [24] is essential among them, which increases the cost and complexity of the fabrication process.

In this letter, we proposed and experimentally demonstrated an easy method to fabricate a miniature Fabry-Perot interferometer (FPI) based on a polymer cap created on the end face of a standard single mode fiber (SMF), which could be used to measure simultaneously surrounding temperature and gas pressure. Such an end-capped FPI sensor exhibits a high pressure sensitivity of ~1130 pm/MPa around the wavelength of 1560 nm, which is three times larger than the formerly reported result8. The FPI sensor also has a high temperature sensitivity based on wavelength shift. Moreover, the proposed device exhibits the advantage of novelty, simplicity, low cost and high sensitivity.

2. Fabrication and experiment

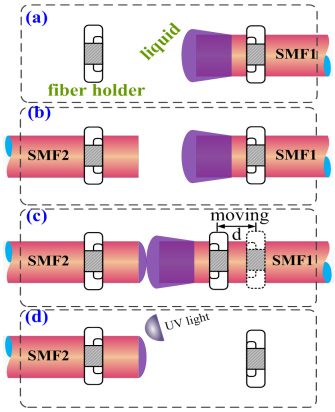

Fig. 1. Schematic diagram of the fabrication process of the FPI sensor.

Figure 1 illustrates the fabrication process of our FPI sensors, which involves four steps. First of all, as shown in Fig. 1(a), the cleaved end of a standard SMF, i.e. SMF1,was immersed into a ultraviolet (UV) curable liquid (NOA65) and then clamped by use of a commercial fusion splicer (Fujikura-60S). It can be found from Fig. 1(a) that some liquid was adhered on the fiber end face and side surface. Secondly, as shown in Figs. 1(b), another cleaved standard SMF, i.e. SMF2, was clamped by the left holder of the splicer. Thirdly, SMF1 was moved toward SMF2 via the motor of the splicer until the liquid adhered on the end face of SMF1 was attached to the endface of SMF2. As a result, some liquid adhered on the endface of SMF2, but no liquid was adhered on the side surface of SMF2. Fourthly, SMF2 was moved away SMF1 and then the liquid adhered on the end face of SMF2 was cured by use of a UV light with an intensity of approximately 270 mW/cm2 for 30 min at room temperature. The liquid, i.e. NOA65, with a refractive index of about 1.51526 was gradually transformed into a solid polymer with a refractive index of 1.524 in the UV-curing process [26,27]. Consequently, a solid polymer cap with a smooth surface was created on the end face of SMF2, as shown in Fig. 1(d) and Fig. 2. Furthermore, the thickness, L, of the polymer cap can be increased by means of repeating the fabrication process above. So we created five polymer cap samples with a thickness of 12.7, 15.8, 23.6, 31.5, and 35.1 μm, respectively.

#222170 - $15.00 USD Received 1 Sep 2014; revised 12 Jan 2015; accepted 19 Jan 2015; published 26 Jan 2015

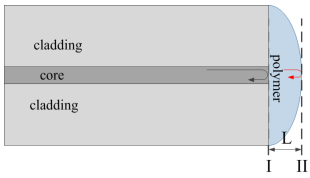

Fig. 2. Schematic diagram of the fiber-tip FPI sensor.

As shown in Fig. 2, such a polymer cap has two interfaces: interface-I between the fiber end and the polymer cap and surface-II between the polymer cap and the surrounding medium. And the reflected lights at the interface-I and interface-II could be collected and guided back to the SMF [28]. Thus the polymer cap could be served as a FPI with a cavity length of *L*, as shown in Fig. 2. A supercontinuum light source (Superk Compact, NKT Photonics) and an optical spectrum analyzer (OSA) (AQ6370C, Yokogawa) were connected to another end of SMF2 via a 3 dB coupler in order to measure the reflection spectrum of the polymer cap. As shown in Fig. 3(a), clear interference fringes were observed in the refection spectra of the polymer-capped FPIs, and total loss in the refection spectrum increases gradually with the increased cavity length, which is contributed to the curvature of the cap. It can be noticed that the radius of curvature of the cap is different for each case, i.e., the cap with the largest L has a smaller radius of curvature, while the thinnest cap has the largest radius of curvature. Moreover, a possibility to explain the losses contribution from the inner low-reflectance surfaces between the layers has been existed.

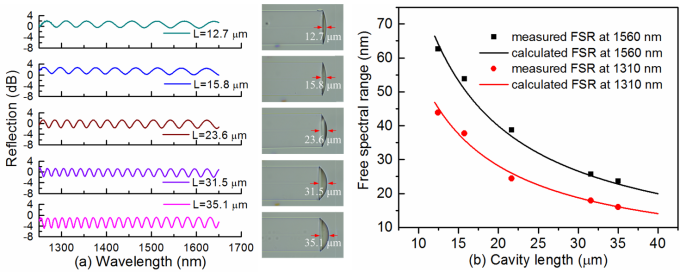

Fig. 3. (a) Reflection spectra and optical microscope images of the five polymer-capped FPIs with different cavity lengths in air at room temperature. (b) Measured and calculated FSR of the FPIs as a function of cavity length around the wavelengths of 1310 and 1560 nm, respectively.

As shown in Fig. 3(b), the free spectral range (FSR) in the reflection spectrum decreases with the increased cavity length. The measured cavity lengths of the five polymer cap samples were 12.7, 15.8, 23.6, 31.5, and 35.1 μm, respectively. Thus, the corresponding FSRs were measured to be ~ 63.9, ~ 51.0, ~ 33.1, ~ 25.4 and ~ 22.7 nm, respectively, around the wavelength of 1560 nm, and to be ~ 43.8, ~ 37.8, ~ 24.3, ~ 17.9 and ~ 15.6 nm, respectively, around the wavelength of 1310 nm. So the measured FSRs agree well with the calculated values by use of Fresnel reflection equation, $FSR=\lambda^2/(2nL)$, where L is the cavity length, n is the refractive index of the cavity, and λ is the dip wavelength.

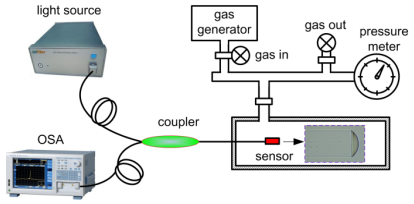

Fig. 4. Experimental setup for measuring the response of the polymer-capped FPI to the gas pressure.

#222170 - $15.00 USD Received 1 Sep 2014; revised 12 Jan 2015; accepted 19 Jan 2015; published 26 Jan 2015

We measured the response of the polymer-capped FPI to the gas pressure by use of the experimental setup consisting of an OSA, a light source and a gas chamber, as shown in Fig. 4. The gas chamber was incorporated with a commercial gas generator and a high-precision pressure meter (ConST-811) which can be used to measure the gas pressure in the chamber. The polymer-capped FPI with a cavity length of 35.1 μm, as shown in Fig. 3(a), was placed into the gas chamber. And then its pigtail fiber and the feed throat of the gas chamber were sealed by strong glue. The reflection spectrum of the polymer-capped FPI was monitored by the OSA while the gas pressure was increased from 0.1 to 2.5 MPa with an increment of 0.4 MPa. Two resonant dips, i.e. DipA and DipB, at a shorter and longer wavelength of 1310 and 1560 nm, respectively, were recorded at different gas pressure. As shown in Fig. 5, both resonant wavelengths of the two interference fringes shifted linearly toward a longer wavelength, i.e. so-called 'red' shift, with the increased gas pressure. But the interference fringe at the shorter wavelength exhibited a lower pressure sensitivity ($S_{pres,A}$) of 978 pm/MPa, in contrast, that at the longer wavelength of about 1560 nm exhibited a higher pressure sensitivity ($S_{pres,B}$) of 1130 pm/MPa. So our polymer-capped FPI could be developed a promising gas pressure sensor.

It should be noted that the pressure response of the polymer cap sample could contribute to the elastic-optic effect and the variation in the length of the cavity, but the form plays a dominant role. As a result, the resonant wavelength of the interference fringes shifted toward to a longer wavelength as the applied gas pressure increased from 0.1 to 2.5 MPa.

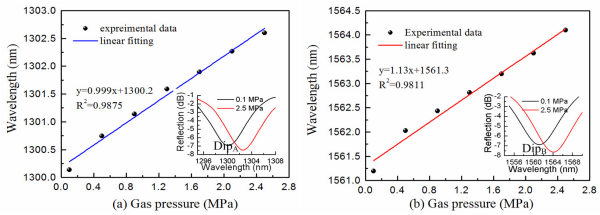

Fig. 5. Resonant wavelengths of the interference fringe at (a) a shorter wavelength of about 1310 nm, i.e. DipA, and (b) a longer wavelength of about 1560 nm, i.e. DipB, versus different gas pressures. The insets show the interference fringes at gas pressure of 0.1 and 2.5 MPa.

Furthermore, the temperature response of the polymer-capped FPI was investigated by placing the device in an electrical oven and gradually increasing the temperature from 40 to 90 °C with an increment of 10 °C. Resonant wavelengths of the two resonant dips, i.e. DipA and DipB, were recorded at different temperature. As shown in Fig. 6, both resonant wavelengths of the two interference fringes shifted linearly toward a longer wavelength with the raised temperature. But the interference fringe at the shorter wavelength exhibited a lower temperature sensitivity ($S_{temp,A}$) of 198 pm/°C, in contrast, that at the longer wavelength of about 1560 nm exhibited a higher temperature sensitivity ($S_{temp,B}$) of 249 pm/°C, which is almost four times higher than that (e.g. about 60 pm/°C) of the conventional long period fiber gratings written in the optical glass fibers [29,30]. So our polymer-capped FPI could be developed a promising temperature sensor.

The temperature response of the polymer cap sample could contribute to the thermal expansion effect and the thermo-optic effect of the polymer employed. For a FPI with a cavity length, i.e. L, the dip wavelength λ_{dip}^{m} is given by:

$$\lambda_{dip}^{m} = \frac{4 \times n_{cavity} \times L}{2m+1}, \mathrm{m} = 0, 1, 2, \ldots \quad (1)$$

where n_{cavity} is the refractive index in the cavity. The temperature sensitivity of the FPI can be given from Eq. (1),

#222170 - $15.00 USD Received 1 Sep 2014; revised 12 Jan 2015; accepted 19 Jan 2015; published 26 Jan 2015

$$\Delta\lambda_{dip}^{m} = \frac{4\times(\alpha + dn/dT)}{2m+1}\times\Delta T \tag{2}$$

where α is the thermal expansion coefficient (225 ppm/°C) of the polymer employed, dn/dT is the thermo-optic coefficient (–1.83 × 10–4 /°C) of the polymer employed [31]. As a result, the calculated temperature sensitivities of the proposed FPI are 220 and 260 pm/°C at the wavelength of 1310 and 1560 nm, respectively. The differences between the calculated temperature sensitivities and the experimental results could owe to the ageing-induced changes in both the thermal expansion coefficient and the thermo-optic coefficient of the polymer employed.

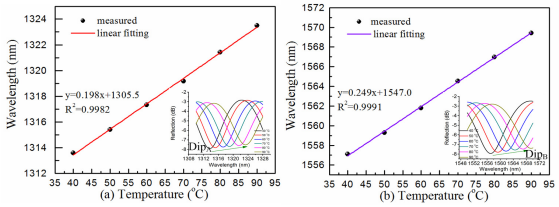

Fig. 6. Temperature response of the dip wavelengths (a) DipA and (b) DipB. The insets in Fig. 6 (a) and Fig. 6 (b) represent the variation of the DipA and the DipB with T ranging from 40 to 90 °C.

As shown in Figs. 5 and 6, the polymer-capped FPI is sensitive to pressure and temperature. But the interference fringe at the longer wavelength has is a higher pressure and temperature sensitivity than that at the shorter wavelength. Hence the cross-sensitivity between pressure and temperature could be solved by the matrix equation below [32]. In other words, the changes of the measured gas pressure and temperature, ΔP and ΔT, can be given by

$$\begin{bmatrix}\Delta T\\ \Delta P\end{bmatrix} = \begin{bmatrix}S_{temp,A} & S_{pres,A}\\ S_{temp,B} & S_{pres,B}\end{bmatrix}^{-1} = -\frac{1}{0.025}\begin{bmatrix}1.13 & -0.978\\ -0.249 & 0.198\end{bmatrix}\begin{bmatrix}\Delta\lambda_A\\ \Delta\lambda_B\end{bmatrix}$$

where ΔT and ΔP are the measured wavelength shift of the interference fringe at the wavelength of about 1310 and 1560 nm, respectively. The temperature-induced error of the pressure measurement is 0.2025 MPa/°C in the case of no temperature compensation. And the pressure-induced error of the temperature measurement is 4.5382 °C/MPa in the case of no pressure compensation.

3. Conclusion

In conclusion, this work proposed a novel polymer-capped FPI and utilizes it to measure the temperature and pressure. Polymer-capped FPI with several cavities were fabricated successfully. The developed device has very favorable characteristics and numerous advantages. We believe that it can be further developed into state-of-the-art of photonic crystal fiber-based fiber sensors where NOA65/NOA61 are mixed with other materials, such as magnetofluids or biochemical materials, to give it a wide range of applications [33,34].

Acknowledgments

This work was supported by National Natural Science Foundation of China/Guangdong (grant nos. 61425007, 11174064, 61377090, and 61308027), Science & Technology Innovation Commission of Shenzhen/Nanshan (grants nos. KQCX20120815161444632, JCYJ20130329140017262, ZDSYS20140430164957664, KC2014ZDZJ0008A), China Postdoctoral Science Foundation funded project (Grant no. 2014M562201) and Pearl River Scholar Fellowships.